Spectrochimica Acta Part A: Molecular and Biomolecular Spectroscopy 95 (2012) 614–621

Contents lists available at SciVerse ScienceDirect

Spectrochimica Acta Part A: Molecular and Biomolecular Spectroscopy

journal homepage: www.elsevier.com/locate/saa

Characterization, photophysical and DFT calculation study on 2-(2,4-difluorophenyl)-1-(4-methoxyphenyl)-1H-imidazo[4,5-f][1,10]phenanthroline ligand

Jayaraman Jayabharathi *, Venugopal Thanikachalam, Marimuthu Venkatesh Perumal

Department of Chemistry, Annamalai University, Annamalainagar 608 002, India

ARTICLE INFO

Article history:
Received 6 February 2012
Received in revised form 4 April 2012
Accepted 10 April 2012
Available online 24 April 2012

Keywords:
Photophysical studies
Multi-component linear regression
DFT calculation
NLO behavior
PES
Electrophilicity index

ABSTRACT

The synthesized imidazole derivative 2-(2,4-difluorophenyl)-1-(4-methoxyphenyl)-1H-imidazo[4,5-f][1,10] phenanthroline (dfpmpip) has been characterized using IR, mass, ^{1}H, ^{13}C NMR and elemental analysis. The photophysical properties of dfpmpip have been studied using UV–visible and fluorescence spectroscopy in different solvents. The solvent effect on the absorption and fluorescence bands has been analyzed by a multi-component linear regression. Theoretically calculated bond lengths, bond angles and dihedral angles are found to be slightly higher than that of X-ray Diffraction (XRD) values of its parent compound. The charge distribution has been calculated from the atomic charges by non-linear optical (NLO) and natural bond orbital (NBO) analysis. Since the synthesized imidazole derivative has the largest $\mu_g\beta_0$ value, the reported imidazole can be used as potential NLO material. The energies of the highest occupied molecular orbital (HOMO) and lowest unoccupied molecular orbital (LUMO) levels and the molecular electrostatic potential (MEP) energy surface studies evidenced the existence of intramolecular charge transfer (ICT) within the molecule. Theoretical calculations regarding the chemical potential (μ), hardness (η) and electrophilicity index (ω) have also been calculated.

Introduction

Phenanthroline derivatives form structural elements of important pharmaceutical drugs such as antimalarial, antifungal, antitumoral, antiallergic, anti-inflammatory and antiviral drugs [1–3] and imidazo[4,5-f][1,10]phenanthroline derivatives have shown interesting proton induced on–off emission switching characteristics [4,5]. 2,9, the 4,7 or the 5,6-di-substituted 1,10-Phenanthroline are used as chelating agents [6,7].

Most π-conjugated systems play a major role in determining second-order NLO response [8]. Benzimidazole based chromophores have received increasing attention due to their distinctive linear, non-linear optical properties and also due to their excellent thermal stability in guest–host systems [9]. The imidazole ring can be easily tailored to accommodate functional groups, which allows the covalent incorporation of the NLO chromophores into polyamides leading to NLO side chain polymers [10].

Our approach is to design a newly π-conjugated phenanthroline derivative to be used as materials in material chemistry [11,12]. The planarity and extension of conjugation of the phenanthroline moiety with imidazole and aryl units lead to an increase of the overall conjugation. Hence there is considerable interest in the synthesis of new materials with optical non-linearity by virtue of their potential use in device applications related to telecommunications, optical computing, optical storage, and optical information processing [13–16]. Herein we report the synthesis, photophysical and theoretical studies of 2-(2,4-difluorophenyl)-1-(4-methoxyphenyl)-1H-imidazo[4,5-f][1,10] phenanthroline (dfpmpip).

Experimental

Computational details

All the calculations are performed with Gaussian 03 [17] package of programs. The geometry of all involved structures is fully optimized with the DFT methodology, using B3LYP/6-31G(d,p) basis set. The molecular electrostatic potential (MEP) of the optimized structures and the representation of HOMO and LUMO orbital density calculations were done at the same level of theory and plotted using Gaussview program.

Spectroscopy

NMR spectrum was recorded on a Bruker 400 MHz NMR instrument using $CDCl_3$ as NMR solvent. The ultraviolet–visible (UV–vis) spectra were measured on a UV–vis spectrophotometer

---

* Corresponding author. Tel.: +91 9443940735.
E-mail address: jtchalam2005@yahoo.co.in (J. Jayabharathi).

1386-1425/$ - see front matter © 2012 Elsevier B.V. All rights reserved.
http://dx.doi.org/10.1016/j.saa.2012.04.059

(Perkin Elmer, Lambda 35) and corrected for background due to solvent absorption at 25.0 ± 0.1 °C in the 200–600 nm spectral range by employing a 1 cm quartz cell, a 1×10^{-5} M solution is used for acquisition. All the fluorescence spectra were recorded on a (Perkin Elmer LS55) fluorescence spectrometer equipped with 1.0 cm quartz cell and the excitation wavelength set was 320 nm. The infrared spectrum was recorded by using KBr pellets on a Avatar 330-Thermo Nicolet FT-IR spectrometer in the 4000–600 cm^{-1} spectral range. Mass spectrum was recorded using Thermo Fischer LC–Mass spectrometer (Plate 1).

Non-linear optical measurements

The second harmonic generation efficiency was assessed by Kurtz powder technique [18] at IISc., Bangalore, India. It is a well established tool to evaluate the conversion efficiency of non-linear optical materials. A Q-switched Nd:YAG laser operating at the fundamental wavelength of 1064 nm, generating about 4.1 mJ and pulse width of 8 ns was used for the present experimental study. The input laser beam was passed through an IR reflector and then incident on the powder form of the specimen, which was packed in a glass capillary tube. The output energy was detected by a photodiode detector integrated with oscilloscope assembly.

Hyperpolarizability calculation

The density functional theory has been used to calculate the dipole moment (μ), mean polarizability (α) and the total first static hyperpolarizability (β) [19] for dfpmpip in terms of x, y, z components and is given by following equations:

$$\mu = \left(\mu_x^2 + \mu_y^2 + \mu_z^2\right)^{1/2} \tag{1}$$

$$\alpha = 1/3(\alpha_{xx} + \alpha_{yy} + \alpha_{zz}) \tag{2}$$

$$\beta_{tot} = \left(\beta_x^2 + \beta_y^2 + \beta_z^2\right)^{1/2}$$

(or)

$$\beta_{tot} = [(\beta_{xxx} + \beta_{xyy} + \beta_{xzz})^2 + (\beta_{yyy} + \beta_{yzz} + \beta_{yxx})^2 + (\beta_{zzz} + \beta_{zxx} + \beta_{zyy})^2]^{1/2} \tag{3}$$

The β components of Gaussian output are reported in atomic units and therefore the calculated values are converted into e.s.u. units (1 a.u. = 8.3693×10^{-33} e.s.u.).

Natural bond orbital (NBO) analysis

The second order Fock matrix was carried out to evaluate the donor–acceptor interactions in the NBO analysis [20]. For each donor (i) and acceptor (j), the stabilization energy $E(2)$ associated with the delocalization $i \rightarrow j$ is estimated as,

$$E(2) = \Delta E_{ij} = q_i \frac{\mathrm{F}(i,j)^2}{\varepsilon j - \varepsilon i} \tag{4}$$

where q_i is the donor orbital occupancy, ε_i and ε_j are diagonal elements and $F(i,j)$ is the off diagonal NBO Fock matrix element. The larger the $E(2)$ value, the more intensive is the interaction between electron donors and electron acceptors.

Synthesis of 2-(2,4-difluorophenyl)-1-(4-methoxyphenyl)-1H-imidazo[4,5-f][1,10] phenanthroline (dfpmpip)

The synthesis of *2-(2,4-difluorophenyl)-1-(4-methoxyphenyl)-1H-imidazo[4,5-f][1,10] phenanthroline* involves a four components assembling [21–23] of a mixture of 1,10-Phenanthroline-5,6-dione (2.10 g, 10 mM), ammonium acetate (2.5 g, 30 mM), 4-methoxyaniline (1.23 g, 10 mM) and 2,4-difluorobenzaldehyde (1.1 ml, 10 mM) in distilled ethanol medium (20 ml) (Scheme 1). The reaction mixture was refluxed at the boiling point of ethanol (78 °C) and the completion of the reaction was monitored by thin layer chromatography (TLC) technique using benzene:ethyl acetate (9:1) as the eluent. The reaction mixture was then extracted with dichloromethane and the resultant resinous material was purified by column chromatography.

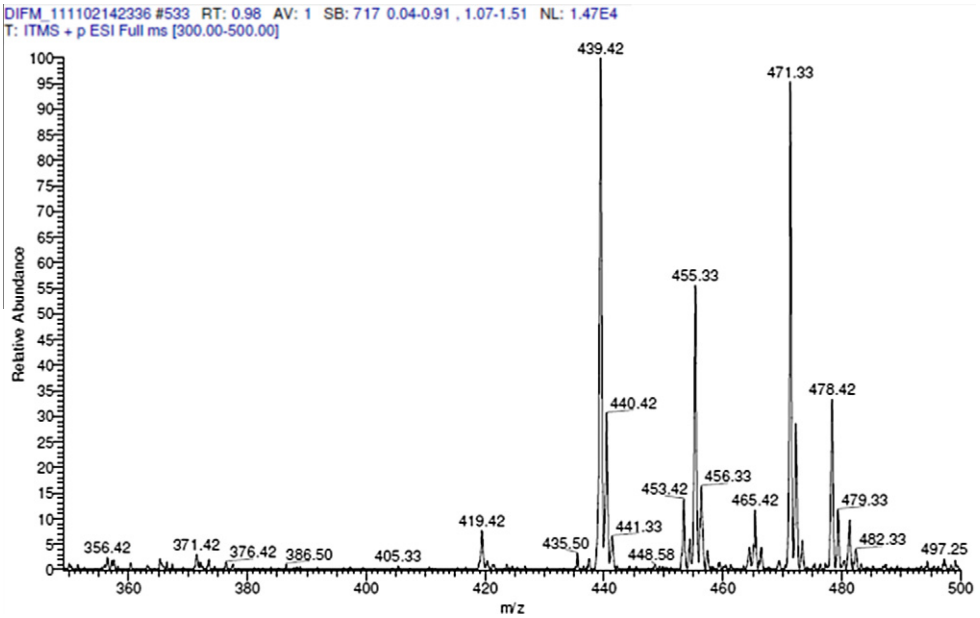

Plate 1. LC–MS spectrum of the imidazole derivative dfpmpip.

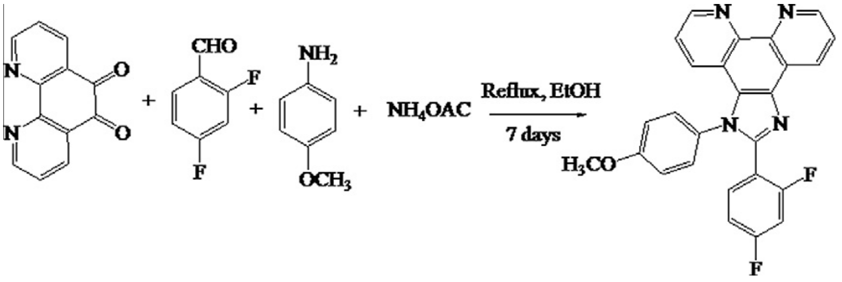

Scheme 1. Synthesis route of dfpmpip.

Results and discussion

Photophysical studies of the imidazole derivative

UV–vis absorption and fluorescence spectral studies have been carried out in different solvents for dfpmpip and the results have been summarized in Table 1. In UV spectral data (Fig. 1), the main absorption band is centered around 270 nm with a high molar absorption coefficient, in addition to this somewhat weaker bands are also observed around 320 nm. The fluorescence spectrum λ_{emi} is centered around 385 nm (Fig. 2).

A multi-parameter correlation analysis [24–27] is employed in which a physicochemical property is linearly correlated with several solvent parameters by means of:

$$(\mathrm{XYZ}) = (\mathrm{XYZ})_0 + \mathrm{C_aA} + \mathrm{C_bB} + \mathrm{C_cC} + \cdots \qquad (5)$$

where $(\mathrm{XYZ})_0$ is the physicochemical property in an inert solvent and $\mathrm{C_a}$, $\mathrm{C_b}$, $\mathrm{C_c}$ and so forth are the adjusted coefficients that reflect the dependence of the physicochemical property (XYZ) on several solvent properties. Solvent properties that mainly affect the photophysical properties of compounds are polarity, H-bond donor capacity and electron donor ability. Different scales for such parameters can be found in the literature, Taft et al. [28] proposed the π^*, α and β scales, whereas more recently Catalan et al. [29] suggested the $\mathrm{SPP^N}$, SA and SB scales to describe the polarity/polarizability, the acidity and basicity of the solvents respectively.

Fig. 3 shows the correlation between the absorption and fluorescence wavenumbers calculated by the multi-component linear regression employing the Taft-proposed solvent parameters and the experimental values. The dominant coefficient affecting the absorption and fluorescence bands of dfpmpip is the polarity/polarizability of the solvent, $C_{\pi*}$ or $C^{\mathrm{N}}_{\mathrm{SPP}}$ having a positive value, corroborating the solvatochromic shifts with the solvent polarity. The coefficient controlling the electron releasing capacity or basicity of the solvent, C_{β} or C_{SB}, is the lowest coefficient (Table 2), hence, the solvent basicity does not play an important role in absorption and fluorescence displacements. The adjusted coefficient representing the acidity of the solvent, C_{α} or C_{SA} has a negative value, suggesting that the absorption and fluorescence bands shift to lower energies with the increasing acidity character of the solvent. This effect can be interpreted in terms of the stabilization of the resonance structures of the chromophore (Fig. S1). The resonance structure "b" bearing negative charge on the carbon atom of the 4-methoxy phenyl ring, so that the structure will be more predominant in acidic solvents because this resonance structure is predominant in the S_1 state and the stabilization of the S_1 state with the solvent acidity would be more important than that of the S_0 state.

Table 1
Photophysical data of dfpmpip in different solvents.

Solvent	Imidazole derivative (1)		
	λ_{abs} (±0.1 nm)	λ_{emi} (±0.4 nm)	$\Delta\upsilon_{ss}$ (cm^{-1})
Hexane	271	375	10,234
1,4-Dioxane	270	380	10,721
Benzene	279	383	9733
Chloroform	273	384	10,588
Ethyl acetate	268	385	11,339
Dichloromethane	271	388	11,127
Butanol	273	396	11,378
Ethanol	270	408	12,527
Methanol	274	410	12,106
Acetonitrile	270	389	11,330
DMSO	269	339	7676
1-Propanol	270	392	11,527

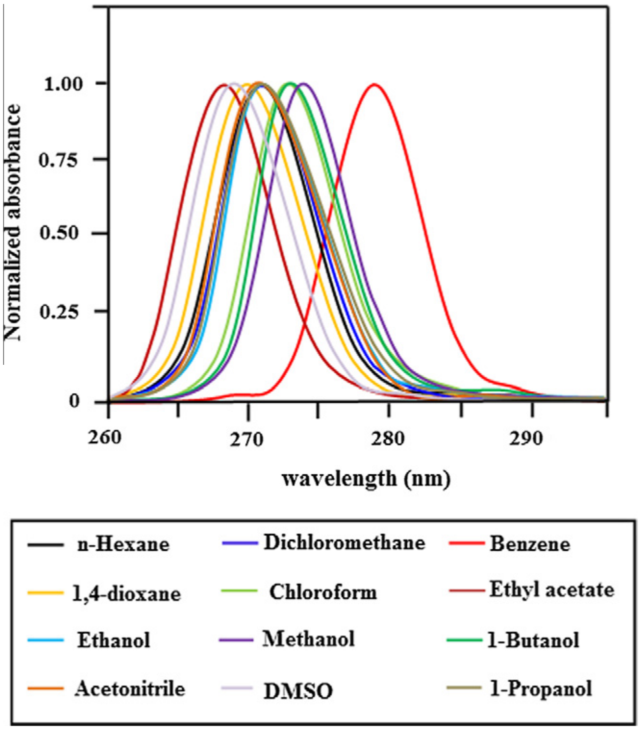

Fig. 1. Absorption spectra of the imidazole derivative in various solvents.

Steric hindrance versus fluorescence quantum yield

DFT calculation reveals that the imidazole ring is essentially planar and makes dihedral angle of 152.40° and 179.73° with the 4-methoxyphenyl and difluorophenyl rings (Fig. S2), respectively. The key twist 'α' is used to indicate the twist of imidazole ring from the aromatic six-membered ring at C(23) (Fig. S3). The α twist originates from the interaction of substituent at N(15) of the imidazole with the substituent at C(23). Emission spectral results reveal that, larger the α twist, the fluorescence quantum yield (0.30) will decrease when compared with its analog compound [30]. Such a

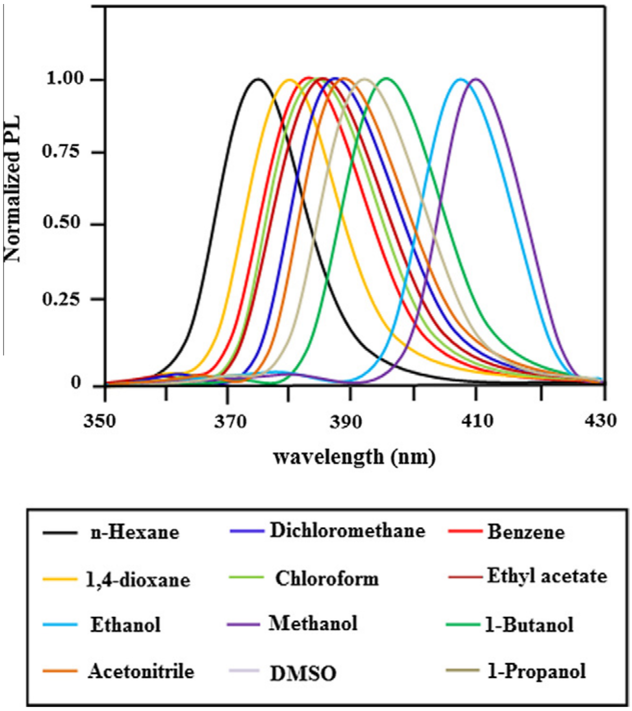

Fig. 2. Emission spectra of the imidazole derivative in various solvents.

clear correlation indicates the importance of coplanarity between imidazole and the aromatic ring at C(23). Since X-ray crystal study of the dfpmpip is currently under progress, its analogous data [31] is taken for comparision. When the two rings are deviated from each other, the *p*-orbital overlapping will be reduced. All these XRD data are in good agreement with the theoretical values. However, from the theoretical values it was found that most of the optimized bond lengths, bond angles and dihedral angles are slightly higher than that of XRD values (Table 3). These deviations can be attributed to the fact that the theoretical calculations were aimed at the isolated molecule in the gaseous phase whereas the XRD results were aimed at the molecule in the solid state.

Potential energy surface (PES) Scan studies

The potential energy surface scan about C20–C22–O45–C46 is performed by using B3LYP/6-31G(d,p) level of theoretical approximation for the compound (dfpmpip). The torsional angle of C20–C22–O45–C46 is also relevant coordinate for conformation flexibility within the molecule. During the calculation all the geometrical parameters were simultaneously relaxed while the C20–C22–O45–C46 torsional angles were varied in steps of 0°,10°,20°,30°,. . .,90°. The potential energy surface diagram (Fig. 4) clearly reveals that the minimum energy (546.6 kcal/mol at 91°) conformation corresponds to the one in which *p*-anisidine ring attached to the nitrogen atom (N15) is tilted to an angle of 92° (about C23–N15–C17–C18) which is in good agreement with the XRD results, whereas the difluoro phenyl ring attached to the carbon atom (C23) is in the angle of 0.27° (about N16–C23–C24–C26). The XRD report for its analog compound shows that the angle is around 55° about N16–C23–C24–C26 [31]. The contraction in theoretical value may be due to the stronger interaction of difluorophenyl ring with the adjacent *p*-anisidine ring attached to the nitrogen atom (N15).

Second harmonic generation (SHG) studies of dfpmpip

Second harmonic signal of 50 mV was obtained for dfpmpip by an input energy of 4.1 mJ/pulse. But the standard KDP crystal gave a SHG signal of 110 mV/pulse for the same input energy. The second order non-linear efficiency will vary with the particle size of the powder sample [32]. Higher efficiencies are achieved by opti-

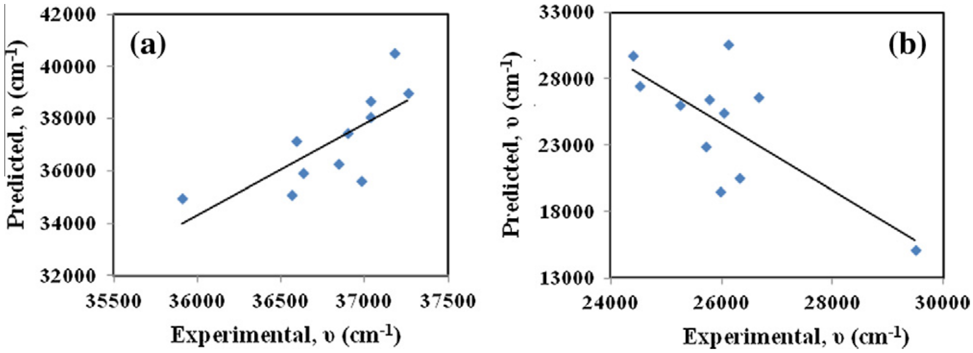

Fig. 3. Correlation between the experimental absorption (a) and fluorescence (b) wavenumber with the predicted values obtained by a multicomponent linear regression using the π*, α and β-scale (Taft) solvent parameters for dfpmpip.

Table 2
Adjusted Coefficients ($(\upsilon_x)_0$, C_a, C_b and C_c) for the multilinear regression analysis of the absorption (υ_{ab}) and fluorescence (υ_{fl}) wavenumbers and stokes shift ($\Delta\upsilon_{ss}$) of the imidazole derivative with the solvent polarity/polarizability, and the acid and base capacity using the Taft (π*, α and β) and the Catalan (SPP^N, SA and SB) scales.

Imidazole derivative (1)				
(υ_x)	$(\upsilon_x)_0$ (cm^{-1})	(π^*)	C_α	C_β
λ_{ab}	$(3.66 \pm 0.021) \times 10^4$	$(2.81 \pm 3.717) \times 10^3$	$-(4.69 \pm 11.964) \times 10^3$	$(2.02 \pm 9.370) \times 10^3$
λ_{fl}	$(2.62 \pm 0.080) \times 10^4$	$-(4.28 \pm 14.456) \times 10^3$	$(12.31 \pm 46.530) \times 10^3$	$-(8.93 \pm 36.440) \times 10^3$
$\Delta\upsilon_{ss} = \upsilon_{ab} - \upsilon_{fl}$	$(1.04 \pm 0.075) \times 10^4$	$(7.09 \pm 13.503) \times 10^3$	$-(16.99 \pm 43.462) \times 10^3$	$(30.95 \pm 34.037) \times 10^3$
		C_{SPP}^{N}	C_{SA}	C_{SB}
λ_{ab}	$(3.68 \pm 0.023) \times 10^4$	$(2.92 \pm 7.797) \times 10^3$	$-(10.39 \pm 32.790) \times 10^3$	$(8.02 \pm 34.459) \times 10^3$
λ_{fl}	$(2.60 \pm 0.055) \times 10^4$	$(25.66 \pm 18.970) \times 10^3$	$-(125.23 \pm 79.777) \times 10^3$	$(129.13 \pm 83.838) \times 10^3$
$\Delta\upsilon_{ss} = \upsilon_{ab} - \upsilon_{fl}$	$(1.08 \pm 0.056) \times 10^4$	$-(22.743 \pm 19.169) \times 10^3$	$(114.83 \pm 80.614) \times 10^3$	$-(121.11 \pm 84.718) \times 10^3$

Table 3
Selected bond lengths, bond angles and torsional angles for dfpmpip.

Bond connectivity	Bond length[a] (Å)	Bond connectivity	Bond angle[a] (°)	Bond connectivity	Torsional angle[a] (°)
C6–C9	1.3710 (1.3770)	C3–C6–C9	121.5689 (123.04)	C3–C6–C9–N16	172.7835 (176.28)
C6–N15	1.4622 (1.3840)	C3–C6–N15	128.7629 (131.74)	C3–C6–N15–C17	43.5222 (−2.3)
C9–N16	1.4666 (1.3789)	C6–C9–N16	109.1597 (111.31)	C3–C6–N15–C23	−165.8720 (−175.82)
N15–C17	1.4700 (1.4402)	C6–N15–C17	113.4900 (128.80)	C6–N15–C17–C18	27.5620 (82.65)
N15–C23	1.4826 (1.3752)	C6–N15–C23	101.2294 (106.40)	C6–N15–C23–C24	−162.3655 (−179.76)
N16–C23	1.3530 (1.3168)	C9–N16–C23	105.3174 (104.52)	N15–C6–C9–N16	7.0381 (−0.78)
C23–C24	1.5400 (1.4782)	N15–C17–C19	120.0021 (119.73)	N15–C23–C24–C25	179.7608 (56.56)
C24–C25	1.3500 (1.3890)	N15–C23–C24	124.0936 (122.78)	N15–C17–C18–C20	−179.9960 (−176.22)
C22–O45	1.4300 (–)	C23–C24–C25	119.9975 (121.16)	N16–C23–C24–C25	0.2420 (−122.35)
C25–F31	1.3500 (–)	C24–C25–F31	119.9997 (–)	C17–N15–C23–C24	−40.2389 (6.4)
C29–F30	1.4300 (–)	C28–C29–F30	120.0004 (–)	C18–C20–C22–O45	180.0000 (–)
O45–C46	1.4014 (–)	C21–C22–O45	120.0024 (–)	C23–C24–C25–F31	−0.0028 (–)
		C22–O45–C46	109.4725 (–)	C26–C28–C29–F30	179.9958 (–)
				C21–C22–O45–C46	90.0284 (–)

[a] Values given in the brackets are corresponding to XRD values of its parent compound [31].

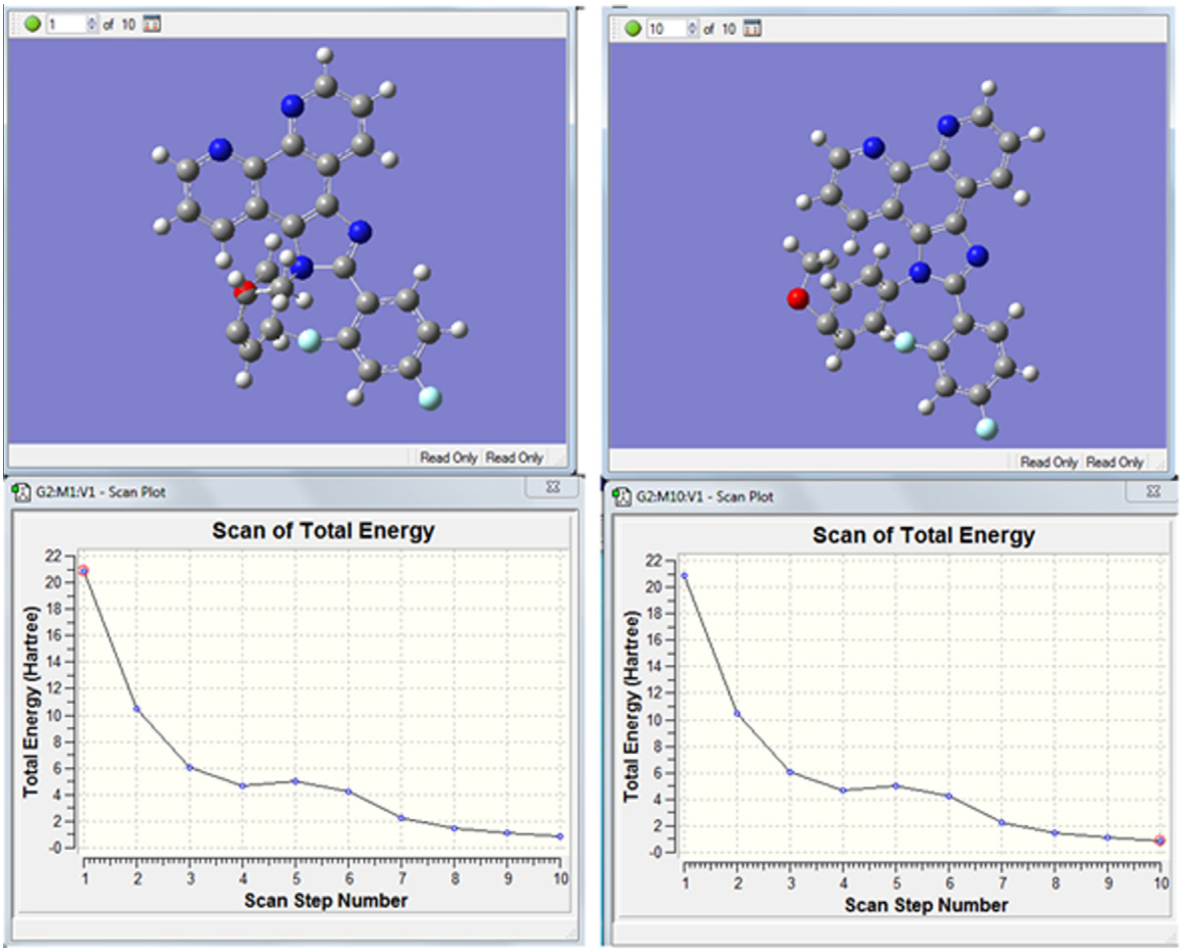

Fig. 4. The potential energy surface (PES) diagram of the imidazole derivative.

mizing the phase matching [33]. On a molecular scale, the extent of charge transfer (CT) across the NLO chromophore determines the level of SHG output, the greater the CT and the larger the SHG output. The ultimate goal in the design of polar materials is to prepare compounds which have their molecular dipole moments aligned in the same direction [34].

Comparison of $\mu\beta_o$

The electrostatic first hyperpolarizability (β) and dipole moment (μ) of the imidazole chromophore have been calculated by using Gaussian 03 package [17]. Theoretical investigation plays an important role in understanding the structure–property relationship, which is able to assist in designing novel NLO chormophores. From Table 4, it is found that the imidazole chromophore show larger $\mu\beta_o$ value, which is attributed to the positive contribution of their conjugation. This chromophore exhibits larger non-linearity and its λ_{abs} is red-shifted when compared with unsubstituted imidazole. Therefore, it is clear that the hyperpolarizability is a strong function of the absorption maximum. Since even a small absorption at the operating wavelength of optic devices can be detrimental, it is important to make NLO chromoph

Table 4
Electric dipole moment (D), polarizability (α) and hyperpolarisability (β_{total}) of dfpmpip.

Parameter	1
Dipole moment (D)	
μ_x	−3.1503
μ_y	3.6150
μ_z	−0.8743
μ_{total}	4.8742
Polarizability (α)	
α_{xx}	−205.9024
α_{xy}	−12.7827
α_{yy}	−160.3089
α_{xz}	9.6128
α_{yz}	−6.7893
α_{zz}	−188.9867
$\alpha \times 10^{-24}$ (esu)	−27.4268
Hyperpolarisability	
β_{xxx}	−84.6523
β_{xxy}	−60.4795
β_{xyy}	24.5416
β_{yyy}	88.0493
β_{xxz}	−20.9547
β_{xyz}	5.1599
β_{yyz}	10.1611
β_{xzz}	−27.4756
β_{yzz}	−4.8360
β_{zzz}	15.2910
$\beta_0 \times 10^{-32}$ (esu)	78.2723
$\mu\beta_0 \times 10^{-32}$ (esu)	381.5148

ores as transparent as possible without compromising the molecule's non-linearity.

The absorption spectrum of dfpmpip was shown in the UV region around 270 nm. The increased transparency in the visible region might enable the microscopic NLO behavior with non-zero values [35–37]. All the absorption bands are due to $\pi \rightarrow \pi^*$ transitions. The β values (Table 4) might be correlated with UV–visible spectroscopic data in order to understand the molecular-structure and NLO relationship in view of a future optimization of the microscopic NLO properties. The band at around 340 nm exhibits a solvatochromic shift, characteristic of a large dipole moment and frequently suggestive of a large hyperpolarizability. This compound show red shift in

Table 5
Significant donor–acceptor interactions of dfpmpip and their second-order perturbation energies (kcal/mol).

Donor (*i*)	*ED*/*e*	Acceptor (*j*)	*ED*/*e*	*E*(2) a.u	*E*(*j*) − *E*(*i*)	*F*(*i*,*j*)
C1–C2	1.9792	C5–N14	0.0125	24.60	0.27	0.073
C3–C4	1.9736	C1–C2	0.0152	20.35	0.28	0.070
C5–N14	1.9853	C3–C4	0.0346	23.49	0.32	0.080
C7–C8	1.9706	C6–C9	0.0239	20.03	0.28	0.069
C10–C11	19.811	C12–N13	0.0128	25.37	0.26	0.074
C12–N13	1.9854	C7–C8	0.0373	22.99	0.32	0.079
C17–C18	1.9761	C19–C21	0.0143	20.42	0.28	0.069
C17–C18	1.9761	C20–C22	0.0276	18.33	0.29	0.065
C19–C21	1.9723	C20–C22	0.0276	20.69	0.28	0.069
C19–C21	1.9723	C17–C18	0.0253	18.64	0.28	0.065
C20–C22	1.9815	C17–C18	0.0253	21.75	0.27	0.069
C20–C22	1.9815	C19–C21	0.0143	20.16	0.28	0.067
C24–C25	1.9775	C26–C28	0.0145	22.00	0.29	0.072
C26–C28	1.9716	C27–C29	0.0270	23.66	0.27	0.072
C27–C29	1.9787	C24–C25	0.0334	22.43	0.29	0.073
LpN15	1.7217	N16–C23	0.0093	21.32	0.34	0.076
LpF30	1.9884	C27–C29	0.0270	21.20	0.42	0.091
LpF31	1.9883	C24–C25	0.0334	21.36	0.41	0.092
C5–N14	1.9854	C1–C2	0.0152	189.01	0.01	0.083
C5–N14	1.9854	C3–C4	0.0346	139.51	0.02	0.082
C12–N13	1.9855	C7–C8	0.0373	153.70	0.02	0.081
C12–N13	1.9855	C10–C11	0.0137	153.12	0.02	0.083
N16–C23	1.9867	C6–C9	0.0249	27.64	0.04	0.055
N16–C23	1.9867	C24–C25	0.0334	134.85	0.01	0.063
C27–C29	1.9787	C26–C28	0.0145	232.79	0.01	0.081

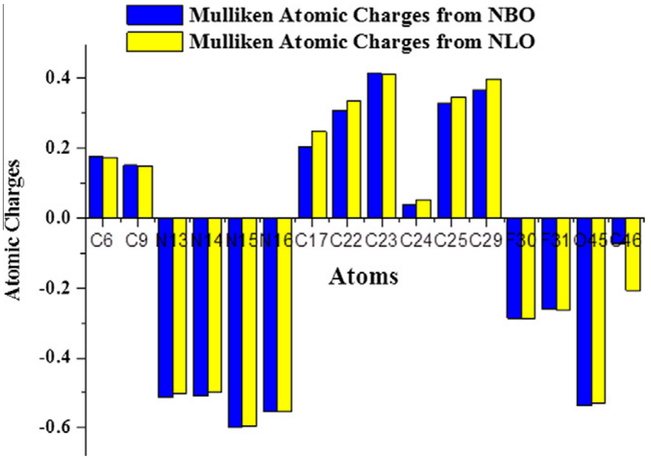

Fig. 5. Bar diagram representing the charge distribution of dfpmpip using NLO and NBO methods.

Table 6
Percentage of s and p-character on each natural atomic hybrid of the natural bond orbital for dfpmpip.

Bond (A–B)	E_D/Energy (a.u.)	ED_A (%)	ED_B (%)	*s* (%)	*p* (%)
C6–C9	0.7080	50.12	49.88	37.26	62.74
	0.7062	–	–	34.81	65.19
C6–N15	0.6183	38.23	61.77	27.04	72.96
	0.7859	–	–	28.50	71.50
C9–N16	0.6520	42.51	57.49	26.58	73.42
	0.7582	–	–	27.20	72.80
N15–C17	0.7819	61.14	38.86	27.23	72.77
	0.6234	–	–	26.42	73.58
N15–C23	0.7912	62.60	37.40	25.45	74.55
	0.6115	–	–	28.72	71.28
N16–C23	0.7647	58.47	41.53	35.10	64.90
	0.6444	–	–	33.57	66.43
C25–F31	0.7042	49.58	50.42	37.60	62.40
	0.7100	–	–	29.17	70.83
C26–F49	0.5291	27.99	72.01	23.13	76.87
	0.8486	–	–	29.49	70.51
C29–F30	0.5252	27.58	72.42	23.09	76.91
	0.8510	–	–	30.21	69.79
C22–O45	0.5818	33.85	66.15	24.54	75.46
	0.8133	–	–	27.08	72.92
O45–C46	0.8216	67.50	32.50	25.06	74.74
	0.5701	–	–	20.71	79.29

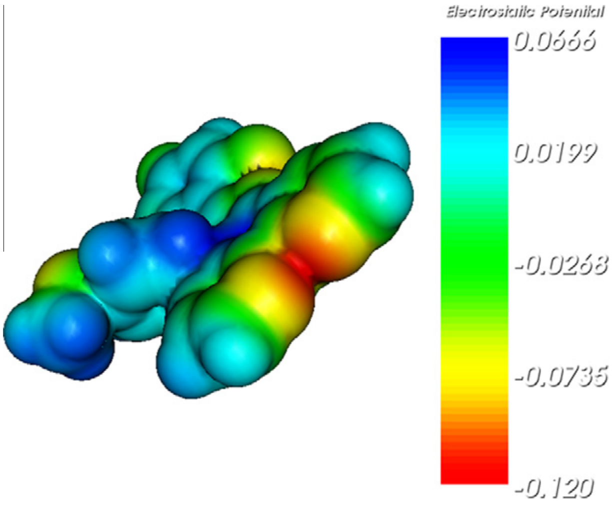

Fig. 6a. MEP surface diagram of dfpmpip.

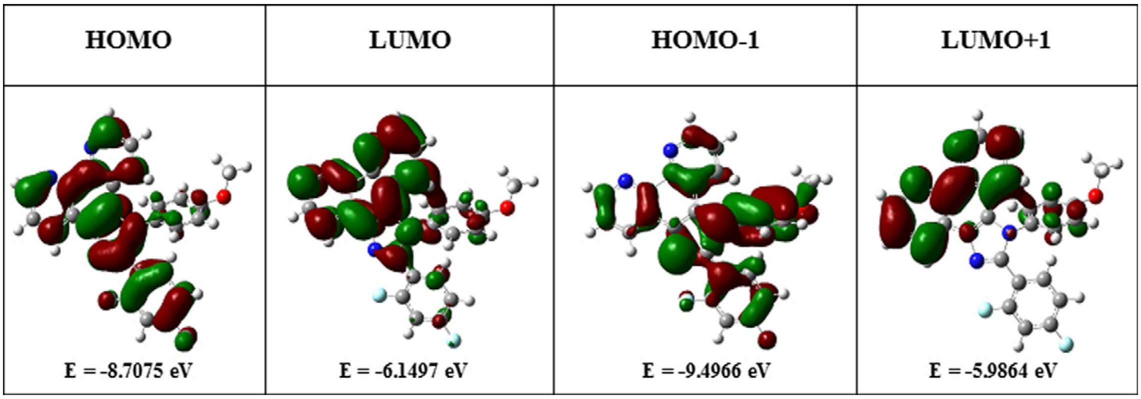

Fig. 6b. HOMO–LUMO energy diagram of dfpmpip.

absorption with increasing solvent polarity, accompanied with the upward shifts non-zero values in the β-components.

β-Tensorial component versus non-linearity

The title compound (dfpmpip) possess a more appropriate ratio of off-diagonal versus diagonal β tensorial component ($r = \beta_{xyy}/\beta_{xxx}$) which reflects the inplane non-linearity anisotropy and the largest $\mu\beta_o$ values.

The β tensor [38] can be decomposed in a sum of dipolar (${}^{j=1}{}_{2D}\beta$) and octupolar (${}^{j=1}{}_{2D}\beta$) tensorial components and the ratio of these two components strongly depends on their 'r' ratios. The zone for $r > r_2$ and $r < r_1$ corresponds to a molecule of octupolar and dipolar respectively. The critical values for r_1 and r_2 are $(1 - \sqrt{3})/\sqrt{3}\sqrt{3} + 1) = -0.16$ and $(\sqrt{3} + 1)/\sqrt{3}(\sqrt{3} - 1) = 2.15$, respectively. Complying with the Pythagorean theory and the projection closure condition, the octupolar and dipolar components of the β tensor can be described as:

$$\|^{j=1}_{2D}\beta\| = (3/4)[(\beta_{xxx} + \beta_{xyy})^2 + [(\beta_{yyy} + \beta_{yxx})^2] \tag{6}$$

$$\|^{j=1}_{2D}\beta\| = (1/4)[(\beta_{xxx} - \beta_{xyy})^2 + [(\beta_{yyy} - \beta_{yxx})^2] \tag{7}$$

The parameter ρ^{2D}, $\rho^{2D} = \frac{\|^{j=3}_{2D}\beta\|}{\|^{j=1}_{2D}\beta\|}]$ is convenient to compare the relative magnitudes of the octupolar and dipolar components of β. The observed positive small ρ^{2D} value (0.386) reveals that the β_{iii} component cannot be zero and these are dipolar component. Since most of the practical applications for second order NLO chromophores are based on their dipolar components, this strategy is more appropriate for designing highly efficient NLO chromophores.

Intramolecular charge transfer from NBO analysis

Several donor–acceptor interactions observed for the imidazole derivative (dfpmpip) have been shown by natural bond orbital (NBO) analysis which have been performed for dfpmpip at the DFT/B3LYP/6-31++G(d,p) level in order to elucidate the intramolecular, delocalization of electron density within the molecule (Tables 5). Among the strongly occupied NBOs, the most important delocalization sites are in the π system and in the lone pairs (n) of the oxygen, fluorine and nitrogen atoms. The important contributions to the delocalization corresponds to the donor–acceptor interactions are C5–N14 → C1–C2, C5–N14 → C3–C4, C12–N13 → C7–C8, C12–N13 → C10–C11, N16–C23 → C6–C9, N16–C23 → C24–C25 and C27–C29 → C26–C28.

The charge distribution of dfpmpip has been calculated from the atomic charges by NLO and NBO analysis (Fig. 5). These two methods predict the same trend i.e., among the nitrogen atoms N15 and N16, N15 is considered as more basic site [36]. The charge distribution shows that the more negative charge is concentrated on N15 atom whereas the partial positive charge resides at hydrogens. When compared to nitrogen atoms (N15 and N16), oxygen and fluorine atoms (F30 and F31) are less electronegative and it can be seen from the bar diagram [39].

The percentage of s and p-character [40] in each NBO natural atomic hybrid orbital are displayed in Table 6. For all the carbon, nitrogen and fluorine atoms, around 70% of p-character and 30% s-character have been observed.

Molecular electrostatic potential map (MEP) and electronic properties

The molecular electrostatic potential surface (MEP) (Fig. 6a) displays molecular shape, size and electrostatic potential values of the imidazole derivative (dfpmpip). MEP surface diagram is used to understand the reactive behavior of a molecule, in that negative regions can be regarded as nucleophilic centers, whereas the positive regions are potential electrophilic sites. The MEP map of dfpmpip shows that the nitrogen, fluorine and oxygen atoms represent the most negative potential region. The hydrogen atoms bear the maximum region of positive charge. The predominance of green region in the MEP surfaces corresponds to a potential halfway between the two extremes red and dark blue color.[1]

The 3D plots of the frontier orbitals HOMO and LUMO of dfpmpip is shown in Fig. 6b. The HOMO is located on the imidazole ring, partly on the phenanthroline ring and on the difluoro phenyl ring, and partly on the carbon atoms of the methoxy phenyl ring. The LUMO is located on the phenanthroline ring, partly on the imidazole ring and on the carbon atoms of both the phenyl rings of the imidazole derivative. The HOMO → LUMO transition implies that intramolecular charge transfer takes place [41] within the molecule. The energy gap (E_g) of dfpmpip has been calculated from the HOMO and LUMO levels. The HOMO–LUMO energy gap supports the probable charge transfer (CD) inside the chromophore.

Electrophilicity index

At the Hatree-Fock level, Koopaman's theorem suggests that the energy of HOMO is good approximation to the negative experimental ionization potential (-IP) [42]. Similarly, it suggests that the electron affinity (EA) for an N-electron system is equal to the negative of the LUMO energy and it is a measure of susceptibility of molecule towards attack by nucleophiles [43]. The dipole mo-

---

[1] For interpretation of color in Figs. 1–6, the reader is referred to the web version of this article.

ment is the most obvious quantity to describe the polarity of a molecule. Electronegativity of imidazole derivative is calculated by,

$$\mu = -\chi = -(\delta E/\delta N)V(r) \tag{8}$$

where E is the energy, N is the number of electrons and $V(r)$ is the constant external potential. By combining the above equation with the work of Ickowski and Margrave [44], assuming a quadrate relationship between E and N and in a finite difference approximation, the equation can be rewritten as,

$$\chi = -\mu = (I + A)/2 \tag{9}$$

$$\chi_{koopaman's} = (E_{\mathrm{HOMO}} + E_{\mathrm{LUMO}})/2 \tag{10}$$

and the global hardness is defined as, $\eta = ½(\delta^2 E/\delta N^2)V(r)$ or $½(E_{\mathrm{HOMO}} - E_{\mathrm{LUMO}})$.

Electrophilicity index of a molecule can be calculated by,

$$\omega = \mu^2/2\eta \tag{11}$$

This electrophilicity index measures the capacity of electrophile to accept the maximal number of electrons in a neighboring reservoir of Electron Sea. By using the above equations, the chemical potential, hardness and electrophicity index have been calculated as $\mu = -0.273$, $\eta = -0.047$ and $\omega = -0.7928$.

Conclusion

We have synthesized and characterized a new imidazole derivative using various spectroscopic techniques. The photophysical properties of the compound have been studied in various solvents and the solvent effect on the absorption and fluorescence bands has been analyzed by a multi-component linear regression in which several solvent parameters were analyzed. Since the acidity of the solvent, C_α or C_{SA} has a negative value, which suggesting that the absorption and fluorescence bands shift to lower energies with the increasing acidity of the solvent. The presence of α twist of the imidazole derivative lowers the fluorescence quantum yield. From the PES scan study, the minimum energy conformation of the molecule is drawn. The observed dipole moment and hyperpolarizability can be explained by the reduced planarity caused by the steric interaction between the two phenyl rings at C(23) and N(15) atoms. Hence, the steric interaction must be reduced in order to obtain larger β_0 values. From the physicochemical studies on imidazoles it was concluded that molecules of higher hyperpolarizability have larger dipole moments used as potential NLO molecules. The electrophilicity index has been calculated in order to measure the capacity of the electrophile to accept the maximal number of electrons in a neighbor reservoir of Electron Sea.

Acknowledgments

One of the authors Dr. J. Jayabharathi is thankful to Department of Science and Technology [No. SR/S1/IC-73/2010], University Grants Commission (F.No. 36-21/2008 (SR)) and Defence Research and Development Organization (DRDO) (F.No. NRB-213/MAT/10-11) for providing funds to this research study.

Appendix A. Supplementary material

Supplementary data associated with this article can be found, in the online version, at http://dx.doi.org/10.1016/j.saa.2012.04.059.

References

[1] J. Pedraza-Chaverri, N. Cardenas-Rodriguez, M. Orozco-Ibarra, J.M. Perez-Rojas, Food. Chem. Toxicol. 46 (2008) 3227.
[2] M.V. Ignatushchenko, R.W. Winter, M. Riscoe, Am. J. Trop. Med. Hgy. 62 (2000) 77.
[3] G. Gopalakrishnan, B. Banumathi, G. Suresh, J. Nat. Prod. 60 (1997) 519.
[4] F. Gao, X. Chen, F. Zhou, et al., Inorg. Chim. Acta 362 (2009) 4960.
[5] F.R. Liu, K.Z. Wang, G.Y. Bai, et al., Inorg. Chem. 43 (2004) 1799.
[6] P.G. Sammes, G. Yahioglu, Chem. Soc. Rev. 23 (1994) 327.
[7] A.R. Katritzky, Q.H. Long, N. Malhotra, T.A. Ramanarayanan, H. Vedage, Synthesis (1992) 911.
[8] C.W. Dirk, H.E. Katz, M.L. Schilling, L.A. King, Chem. Mater. 2 (1990) 700.
[9] E.M. Across, K.M. White, R.S. Moshrefzadeh, C.V. Francis, Macromolecules 28 (1995) 2526.
[10] X.R. Bu, H. Li, D.V. Derveer, E.A. Mintz, Tetrahedron Lett. 37 (1996) 7331.
[11] C.R. Moylan, R.D. Miller, R.J. Twieg, K.M. Betterton, V.Y. Lee, T.J. Matray, C. Nguyen, Chem. Mater. 5 (1993) 499.
[12] M. Ammamm, P. Bauerle, Org. Biomol. Chem. 3 (2005) 4143.
[13] S.R. Marder, J.E. Sohn, G.D. Stucky (Eds.), Materials for Non-linear Optics: Chemical Perspectives. In: ACS Symposium Series, vol. 455, American Chemical Society, Washington, DC, 1991.
[14] J. Messier, F. Kajzar, P. Prasad (Eds.), Organic Molecules for Non-linear Optics and Photonics, Kluwer Academic, Dordrecht, 1991.
[15] L.R. Dalton, A.W. Harper, R. Ghosn, W.H. Steir, M. Ziari, H. Fetterman, Y. Shi, R.V. Mustacich, A.K.Y. Jen, K.J. Shea, Chem. Mater. 7 (1995) 1060.
[16] R.G. Benning, J. Mater. Chem. 5 (1995) 365.
[17] M.J. Frisch, G.W. Trucks, H.B. Schlegel, G.E. Scuseria, M.A. Robb, J.R. Cheeseman, J.A. Montgomery, T. Vreven Jr., K.N. Kudin, J.C. Burant, J.M. Millam, S.S. Iyengar, J. Tomasi, V. Barone, B. Mennucci, M. Cossi, G. Scalmani, N. Rega, G.A. Petersson, H. Nakatsuji, M. Hada, M. Ehara, K. Toyota, R. Fukuda, J. Hasegawa, M. Ishida, T. Nakajima, Y. Honda, O. Kitao, H. Nakai, M. Klene, X. Li, J.E. Knox, P. Hratchian, J.B. Cross, C. Adamo, J. Jaramillo, R. Gomperts, R.E. Stratmann, O. Yazyev, A.J. Austin, R. Cammi, C. Pomelli, J.W. Ochterski, P.Y. Ayala, K. Morokuma, G.A. Voth, P. Salvador, J.J. Dannenberg, V.G. Zakrzewski, S. Dapprich, A.D. Daniels, M.C. Strain, O. Farkas, D.K. Malick, A.D. Rabuck, K. Raghavachari, J.B. Foresman, J.V. Ortiz, Q. Cui, A.G. Baboul, S. Clifford, J. Cioslowski, B.B. Stefanov, G. Liu, A. Liashenko, P. Piskorz, I. Komaromi, R.L. Martin, D.J. Fox, T. Keith, M.A. Al-Laham, C.Y. Peng, A. Nanayakkara, M. Challacombe, P.M.W. Gill, B. Johnson, W. Chen, M.W. Wong, C. Gonzalez, J.A. Pople, Gaussian 03, Revision C.02, Gaussian, Inc., Wallingford, CT, 2004.
[18] S.R. Flom, P.F. Barbara, Chem. Phys. Lett. 94 (1983) 488.
[19] M. Wagener, J. Sadowsky, J. Gasteiger, J. Am. Chem. Soc. 117 (1995) 7769.
[20] Y. Yang, W.J. Zhang, X.M. Gao, Int. J. Quantum Chem. 106 (2006) 1199–1207.
[21] .S. Rosepriya, M. Venkatesh Perumal, A. Thiruvalluvar, J. Jayabharathi, R.J. Butcher, J.P. Jasinski, J.A. Golen, Acta Cryst. E67 (2011) o1965.
[22] .J. Jayabharathi, V. Thanikachalam, M. Venkatesh Perumal, N. Srinivasan, Spectrochim. Acta Part A 79 (2011) 236.
[23] J. Jayabharathi, V. Thanikachalam, M. Venkatesh Perumal, K. Saravanan, J. Fluoresc. (2011), http://dx.doi.org/10.1007/s10895-011-0878-3.
[24] Y. Marcus, Chem. Soc. Rev. 22 (1993) 409.
[25] C. Reichardt, Chem. Rev. 94 (1994) 2319.
[26] E. Lippert, in: J.B. Birks (Ed.), Organic Molecular Photophysics, vol. 2, Wiley-Interscience, Bristol, England, 1975, p. 1.
[27] K. Dimroth, C. Reichardt, Liebigs Ann. Chem. 727 (1969) 93.
[28] M.J. Kamlet, R.W. Taft, J. Am. Chem. Soc. 98 (1976) 377.
[29] J. Catalan, V. Lopez, P. Perez, J. Fluoresc. 6 (1996) 15.
[30] J. Jayabharathi, V. Thanikachalam, M. Venkatesh Perumal, N. Srinivasan, J. Fluoresc. (2011), http://dx.doi.org/10.1007/s10895-011-1009-x.
[31] S. Rosepriya, A. Thiruvalluvar, J. Jayabharathi, M. Venkatesh Perumal, R.J. Butcher, J.P. Jasinski, J.A. Golen, Acta Cryst. E67 (2011) o989.
[32] Y. Porter, K.M. OK, N.S.P. Bhuvanesh, P.S. Halasyamani, Chem. Mater. 13 (2001) 1910.
[33] M. Narayana Bhat, S.M. Dharmaprakash, J. Cryst. Growth 236 (2002) 376.
[34] D. Steiger, C. Ahlbrandt, R. Glaser, J. Phys. Chem. B 102 (1998) 4257.
[35] V. Crasta, V. Ravindrachary, R.F. Bharantri, R. Gonsalves, J. Cryst. Growth 267 (2004) 129.
[36] P. Wang, P. Zhu, W. Wu, H. Kang, C. Ye, Phys. Chem. Chem. Phys. 1 (1999) 3519.
[37] Y. Yang, W.J. Zhang, X.M. Gao, Int. J. Quant. Chem. 106 (2006) 1199.
[38] S.F. Tayyari, S. Laleh, Z.M. Tekyeh, M.Z. Tabrizi, Y.A. Wang, H. Rahemi, Mol. Struct. 827 (2007) 176.
[39] G. Wang, F. Lian, Z. Xie, G. Su, L. Wang, X. Jing, F. Wang, Synth. Met. 131 (2002) 1.
[40] M. Szafran, A. Komasa, E.B. Adamska, J. Mol. Struct. 827 (2007) 101.
[41] K. Fukui, T. Yonezawa, H. Shingu, J. Chem. Phys. 20 (1952) 722.
[42] L.J. Bellamy, The infrared Spectra of Complex Molecules, vol. 2, Chapman and Hall, London, 1982.
[43] R.G. Parr, R.A. Donnelly, M. Levy, W.E. Palke, J. Chem. Phys. 68 (1978) 3801.
[44] R.P. Iczkowski, J.L. Margrave, J. Am. Chem. Soc. 83 (1961) 315.